Published in final edited form as:
Dev Dyn. 2013 September ; 242(9): 1101–1109. doi:10.1002/dvdy.23990.

Nuclear phosphatase PPM1G in cellular survival and neural development

William H. Foster[1,2], **Adam Langenbacher**[3], **Chen Gao**[2], **Jaunian Chen**[3], and **Yibin Wang**[1,2]

[1]Molecular, Cellular and Integrated Physiology Program, University of California at Los Angeles, Los Angeles, CA 90095

[2]Division of Molecular Medicine, Department of Anesthesiology, Medicine and Physiology, University of California at Los Angeles, Los Angeles, CA 90095

[3]Department of Molecular, Cell and Developmental Biology, University of California at Los Angeles, Los Angeles, CA 90095

Abstract

Background—PPM1G is a nuclear localized serine/threonine phosphatase implicated to be a regulator of chromatin remodeling, mRNA splicing and DNA damage. However, its *in vivo* function is unknown.

Results—Here we show that ppm1g expression is highly enriched in the central nervous system during mouse and zebrafish development. *ppm1g*$^{-/-}$ mice were embryonic lethal with incomplete penetrance after E12.5. Rostral defects, including neural tube and craniofacial defects were observed in *ppm1g*$^{-/-}$ embryos associated with increased cell death in the neural epithelium. In zebrafish, loss of *ppm1g* also led to neural defects with aberrant neural marker gene expression. Primary fibroblasts from *ppm1g*$^{-/-}$ embryos failed to grow without immortalization while immortalized *ppm1g*$^{-/-}$ fibroblasts had increased cell death upon oxidative and genotoxic stress when compared to wild type fibroblasts.

Conclusion—Our *in vivo* and *in vitro* studies revealed a critical role for PPM1G in normal development and cell survival.

Keywords

PPM1G; neural tube; serine threonine phosphatase; PP2Cγ

Introduction

Type 2C phosphatase family (PP2C or PPM)(Guthridge et al., 1997; Travis and Welsh, 1997; Murray et al., 1999) have been implicated in cellular stress responses(Lu and Wang,

Correspondence: Yibin Wang, Ph.D., Departments of Anesthesiology, Physiology and Medicine, BH-569, CHS, University of California, Los Angeles, Los Angeles, CA 90095, Tel: 310-206-5197; Fax: 310-206-5907, yibinwang@mednet.ucla.edu.

Competing Interests: The authors have declared no competing interest

Authorship Contributions: WF and YW conceived and designed the experiments. WF, AL and CG aonducted the experiments. WF, AL, CG, JC and YW analyzed data WF AL CG JC YW. WF and YW wrote the manuscript.

2008). All PPM phosphatases share a conserved pp2c domain and many display specific sub-cellular localization(Stern et al., 2007). The most extensively studied PPMs, PPM1A and PPM1B are located in the cytosol(Lu and Wang, 2008), while three other members: PPM1D, PPM1G (*pp2cγ*) and PPM1M are all located in nuclei(Komaki et al., 2003). The PPM1D coding gene *ppm1d* is an established oncogene amplified in breast cancer(Li et al., 2002) and PPM1M function is unknown.

PPM1G is a PP2C family member with a unique acidic domain inserted in the middle of the conserved PP2C phosphatase domain which may direct substrate specificity(Travis and Welsh, 1997; Murray et al., 1999). *In vitro* work has implicated PPM1G in diverse nuclear functions including mRNA splicing(Murray et al., 1999; Allemand et al., 2007), snRNP assembly(Petri et al., 2007), Histone exchange(Kimura et al., 2006) and DNA damage and repair(Kimura et al., 2006; Beli et al., 2012; Khoronenkova et al., 2012). However, the *in vivo* function of PPM1G remains unknown.

Here we employed *ppm1g*$^{-/-}$ mice and *ppm1g* morphant zebrafish as animal models to investigate the *in vivo* function of PPM1G during vertebrate development. We found that *ppm1g* expression was wide-spread but enriched in the neural epithelium along the neural tube during embryonic development. Significant embryonic lethality was observed in *ppm1g*$^{-/-}$ embryos associated with augmented apoptosis in the mesencephalon and metencephalon as well as elevated stress signaling. *ppm1g* inactivation in zebrafish also led to rostral neural defects and elevated cell death in the central nervous system. In addition, we found mouse embryonic fibroblasts (MEFs) derived from the *ppm1g*$^{-/-}$ embryos fail to grow without SV40 immortalization and the immortalized *ppm1g*$^{-/-}$ MEF cells were more susceptible to stress induced cell death when compared to wild type MEFs. All these results suggest that PPM1G is critical for cellular growth and survival in response to stress and has a conserved and essential role in vertebrate neural development.

Results

ppm1g gene is highly expressed across neural structures in developing embryos

The *ppm1g*$^{+/-}$ mice were obtained from Deltagen in which one allele carrying a *lacZ neomycin* fusion gene replacing portions of *ppm1g* exons 4 and 5 by homologous recombination (Figure 1A for schematic illustration and genomic PCR) and were backcrossed into C57BL6 background. The *ppm1g*$^{-/-}$ had a complete loss of *ppm1g* expression as demonstrated at mRNA level by qRT-PCR on samples from whole embryos (Figure 1B) and at protein level by immunoblot on samples from derived mouse embryonic fibroblasts (Figure 1C). Since the lacZ/neomycin cassette was fused in-frame into the *ppm1g* coding sequence, the expression pattern of the *ppm1g* gene could be revealed via X-gal staining in the *ppm1g*$^{+/-}$ embryos. At E8.5, positive LacZ staining was detected mostly along the neural plate and the neural folds (Figure 2A, E). This expression persisted throughout the length of the neural tube in E9.5, E10.5 and E12.5 embryos (Figure 2). LacZ staining in the E9.5 embryos indicated that *ppm1g* is broadly expressed at high levels in neural regions including the hindbrain, midbrain, otic vesicle, and somites (Figure 2B, F). In E10.5 embryos, there was strong expression in the first two branchial arches, the frontal nasal process and the telencephalon. Additional LacZ signal was also present in the

midbrain and hindbrain areas (Figure 2C, G). The limb buds at this stage were also strongly stained, with additional expression present in somites and weak expression in the heart. The E12.5 embryos revealed that *ppm1g* is expressed in most rostral structures including the maxilla, mandible, and neck regions (Figure 2I). Sections of E10.5 embryos revealed that *ppm1g* was expressed within the neural ectoderm without detectable expression in the cephalic mesenchyme (Figure 2D, H). These data indicate that *ppm1g* expression in the developing embryo is enriched in neural structures. LacZ activities from adult $ppm1g^{+/-}$ mice was also measured utilizing the CPRG assay, which detected a high level of expression in the testes, small intestine, brain and spleen (Supplemental Figure 1A).

$ppm1g^{-/-}$ mice are embryonic lethal

Only one $ppm1g^{-/-}$ mouse was obtained at weaning from all the crosses between heterozygous $ppm1g^{+/-}$ mice (0.72%, 1/138). Between E8.5–E12.5, the number of surviving $ppm1g^{-/-}$ embryos became progressively lower than the expected Mendelian ratios (21.4, 20.7, 16.4 and 15.5% respectively) (Table 1). From embryonic stages after E13.5 until P0, the majority of $ppm1g^{-/-}$ embryos did not survive (7/304). Clearly, *ppm1g* deficiency leads to embryonic lethality between E12.5–E13.5.

$ppm1g^{-/-}$ embryos have rostral defects

Rostral neural tube defects were observed in 27.8% (5/18) of the $ppm1g^{-/-}$ embryos between E12 and E14.5. Shown in Figure 2 are several defects observed in the $ppm1g^{-/-}$ embryos including open neural tubes and exencephaly. At E14.5, we found that one surviving $ppm1g^{-/-}$ embryo had a severe rostral defect with failed neural tube closure (Figure 2O). Therefore, consistent with its enriched expression pattern, significant defects were observed in the developing neural tube of the $ppm1g^{-/-}$ mouse embryos.

The surviving $ppm1g^{-/-}$ adult has a craniofacial defect

We observed only one $ppm1g^{-/-}$ mouse from all the heterozygous crossings survived beyond birth and weaning. This $ppm1g^{-/-}$ mouse was severely runted and failed to grow at the same rate as the littermates (Supplemental Figure 2A). This mouse also exhibited circling behavior, suggestive of a neural defect. At 2 months of age, this mouse was euthanized due to lack of growth. Upon necropsy, it was observed that the $ppm1g^{-/-}$ mouse had craniofacial defects such as a deviated maxilla (Supplemental Figure 2B).

Loss of *ppm1g* leads to increased apoptosis of E9.5 and 10.5 midbrain and hindbrain neural epithelium

To determine whether a change in proliferation or cell death occurred in the $ppm1g^{-/-}$ embryos, we performed immunohistochemistry for phosphorylated histone H3 serine 10 (H3P) and TUNEL staining. The distribution of proliferating cells in E10.5 brain was mostly observed at ventricle side as expected in both wild type and $ppm1g^{-/-}$ mice with no significant differences (Figure 3). In contrast, a significant increase in TUNEL positive apoptotic cells was observed in the midbrain neural epithelium of E9.5 and E10.5 $ppm1g^{-/-}$ embryos (Figures 4 and 5). The level of apoptosis was highest in the rostral portion of the hindbrain (Figure 5E), while the neural tube at the level of rhombomeres 4 and 5 showed

similar levels of apoptosis when compared to wildtype controls (Figure 4). This indicates that apoptotic events in *ppm1g*$^{-/-}$ embryos are concentrated around the rostral neural tube, particularly around the midbrain and hindbrain. In addition to apoptosis, we cannot exclude other forms of cell death, such as necrosis, are also implicated in the abnormalities observed in *ppm1g*$^{-/-}$ embryos.

ppm1g$^{-/-}$ embryos have increased stress signaling

As *ppm1g*$^{-/-}$ embryos had increased cell death in the neural epithelium, we examined whether there was also a change in pro-apoptotic stress signaling pathways. Immunoblot analysis of E10.5 wild type, *ppm1g*$^{+/-}$ and *ppm1g*$^{-/-}$ embryos revealed an increase in the stress activated protein kinase activity in *ppm1g*$^{-/-}$ embryos as demonstrated by the higher levels of phospho-p38 MAPK when compared to wild type or heterozygous embryos (Figure 5F).

ppm1g's function in zebrafish neural development

The *ppm1g* gene is highly conserved in vertebrates based on peptide sequence alignment among human, mouse, chicken and zebrafish (Supplemental Figure 3). By in-situ hybridization in zebrafish egg and embryos, *ppm1g* mRNA was detected ubiquitously at the onset of gastrulation (Figure 6A) but became more restricted to the central nervous system and posterior somites, spinal cord (motoneurons) and floor plate as somitogenesis proceeds (Figure 6B,C). By 24 hours post fertilization (hpf), *ppm1g* mRNA was strongly detected in the brain, spinal cord, eyes, and branchial arches (Figure 6D, lateral; E, dorsal). At 48 hpf, *ppm1g* expression remained strong in the brain, eyes, and branchial arches (Figure 6F). Overall, these observations were largely consistent with what were reported by Thisse *et al*(Thisse et al., 2004). Therefore, the enriched expression of *ppm1g* in the central nervous system during embryonic development appears to be conserved in vertebrates.

To investigate the functional role of *ppm1g* in zebrafish, we established *ppm1g* knockdown fish using specific morpholino targeting the zebrafish homolog of *ppm1g*. Compared to control zebrafish or zebrafish injected with a random morpholino (Supplemental Figure 4), the *ppm1g* morphants showed central nervous system defects, with smaller heads and underinflated midbrain ventricles at 36 hours post fertilization (hpf) (Figure 7A, B). Also, there was elevated cell death in the forebrain ventricular zone, and the rest of the central nervous system, including the midbrain, hindbrain, and spinal cord (Figure 7C, D, Supplemental Figure 4C). Additionally, the *ppm1g* morphants exhibited abnormal expression of neural markers. In *ppm1g* morphants, the *pax2* expression was extended anteriorly beyond the midbrain/hindbrain boundary to include the midbrain tectum (Figure 7G). Increased *pax2* expression was also detected in the choroid fissure and optic nerve of *ppm1g* morphants (Figure 7G). Similarly, the expression level of *notch1B* was increased in the brains of the 48 hpf old *ppm1g* morphants compared to the controls (Figure 7H, I). Overall, *ppm1g* morphants exhibited abnormal neural marker expression patterns and neural defects associated with elevated cell death. Therefore, PPM1G has a conserved function in neural development and cell survival in vertebrates.

PPM1G regulates cellular survival and stress response *in vitro*

To explore the cellular effects of *ppm1g* function *in vitro*, MEF cells were derived from E10.5 embryos from wild type, *ppm1g*$^{+/-}$ and *ppm1g*$^{-/-}$ embryos. The genotyping and deficiency in Ppm1g protein expression were confirmed by genomic PCR and immunoblot (Figure 1). Primary MEFs from the heterozygous and wild type embryos were readily established and expanded in cell culture. However, primary MEFs from *ppm1g*$^{-/-}$ embryos failed to propagate beyond the second passage (from 24 well plates to a single 6 well plate) (Supplemental Table 1). Therefore, only immortalized wild type and *ppm1g*$^{-/-}$ MEFs were used for the following studies.

As PPM1G is reported to be a key regulator in ATM mediated regulation of DNA damage response(Khoronenkova et al., 2012) and apoptosis, and our *ppm1g*$^{-/-}$ embryos displayed elevated apoptosis and stress signaling, we tested the viability of MEFs in response to DNA damaging and oxidative stress. Genotoxic stress was tested with the topoisomerase inhibitor doxorubicin (DOX at 1μM) and oxidative stress was tested by hydrogen peroxide (H_2O_2, at 50 μM). There was significantly increased cell death in *ppm1g*$^{-/-}$ MEFs compared to wild type controls following H_2O_2 treatment (Figure 8 C–F). Conversely Hela cells overexpressing PPM1G were less sensitive to H_2O_2 induced cell death (Supplemental Figures 5,6). As shown in Figure 8E, in response to treatment with Dox or H_2O_2, the cell viability of the *ppm1g*$^{-/-}$ MEFs was significantly lower than the wild type control ($p < 0.05$). This response was replicated in independently derived *ppm1g*$^{-/-}$ MEF and wildtype MEF lines (Supplemental Figure 6). These data suggest that PPM1G regulates stress induced cell death.

We further determined whether there was an increase in stress signaling in the *ppm1g*$^{-/-}$ MEFs. Serum starved (2% FBS, 1% P/S DMEM) wild type and *ppm1g*$^{-/-}$ MEFs were subjected to Dox for 0–12 hours and examined for phosphorylation levels of the stress activated MAP kinases, p38 (Figure 8G). The *ppm1g*$^{-/-}$ MEFs have a more pronounced activation of p38 activity over the course of 12 hours when compared to wildtype MEFs.

Discussion

PPM1G was reported to regulate DNA damage response (Kimura et al., 2006; Beli et al., 2012; Khoronenkova et al., 2012) and histone exchange(Kimura et al., 2006) based on *in vitro* studies. However the *in vivo* role of PPM1G remained completely unknown. Here we show for the first time that PPM1G expression is highly enriched in embryonic neural tissues and is important for the survival of the developing embryo. In the *ppm1g* deficient embryos, neural tube defects were observed alongside elevated neural apoptosis and increased stress signaling. The *ppm1g*$^{-/-}$ MEFs also showed an increased susceptibility to stress induced cell death and stress signaling response. PPM1G's role in cranial and neural development is best illustrated by the conservation of PPM1G's function in zebrafish. In *ppm1g* morphants, there were rostral defects including ventricle under inflation, increased cell death and dysregulation of the hindbrain markers pax2 and notch1B. Overall, our data has revealed the *in vivo* expression pattern and the functional importance of *ppm1g* during neural development and demonstrated an important function for PPM1G in cell death regulation during development and genotoxic stress.

It is not entirely clear what constitutes the underlying mechanisms for the neural tube defects observed in the *ppm1g*$^{-/-}$ embryos. PPM1G was found to interact with and regulate an alternative splicing factor YB1(Allemand et al., 2007). Interestingly, the *yb1*$^{-/-}$ mice also have neural tube defects as well as deficiency in cell growth(Uchiumi et al., 2006). Neural tube defects were also reported in the double knockouts for both *yb1* and *msy4* gene(Lu et al., 2006). Therefore, it would be worthwhile to investigate whether the loss of YB1 dephosphorylation and subsequent loss of proper YB1 mediated mRNA splicing contribute to the embryonic lethality and neural tube defects found in the *ppm1g*$^{-/-}$ mice.

Another reported target of PPM1G is SMN which modulates the nuclear/cytoplasmic transport for snRNP assembly and localization(Petri et al., 2007). Human SMN mutations cause a loss of motor neuron function and muscle weakness ranging from mortality to mild weakness(Humphrey et al., 2011), while deletion or catalytic defective mutants of SMN1 in mice result in defects in axonal growth(Rossoll et al., 2003; Gabanella et al., 2005). However these are not as severe or early as the embryonic lethality observed in the *ppm1g*$^{-/-}$ embryos. Therefore, SMN phosphorylation defects may not represent the full spectrum of the downstream effects due to *ppm1g* inactivation.

Kimura et al., found that PPM1G directly bound histones H2A/H2B, and that PPM1G could dephosphorylate H2B ser14, H2A ser1, and γH2AX ser139 residues in response to DNA damage (Kimura et al., 2006). Other recent work also indicated that PPM1G may have a role in the DNA damage response downstream of ATM(Kimura et al., 2006; Beli et al., 2012; Khoronenkova et al., 2012). Beli et al. found that PPM1G was phosphorylated in response to DNA damage and recruited to the γH2AX foci of DNA damage in response to topoisomerase inhibition. Previous studies indicated that PPM1G overexpression impaired cell cycle progression(Suh et al., 2009), while knockdown of PPM1G with siRNA also lead to a proliferative defect(Allemand et al., 2007; Khoronenkova et al., 2012). Indeed, *ppm1g*$^{-/-}$ MEFs showed an inability to divide without immortalization which is consistent with the senescence phenotype observed in the MEFs with deficient DNA damage response, such as Ku70$^{-/-}$, Ku80$^{-/-}$ and ATM$^{-/-}$ MEFs (Elson et al., 1996; Nussenzweig et al., 1996; Gu et al., 1997). However, our *in vivo* analysis did not detect any significant differences in cell proliferation between the wildtype and the *ppm1g* deficient embryos. Therefore, it is unlikely that the developmental phenotype observed in the *ppm1g*$^{-/-}$ embryos is a direct result of defects in cell proliferation.

Embryos deficient for *ppm1g* had increased cell death as well as activation of stress kinase p38. To assess whether the increased cell death and stress activation was a cell autonomous effect in the *ppm1g* deficient cells, we analyzed stress induced cell death in the immortalized *ppm1g*$^{-/-}$ MEFs. Compared to wild type MEFs, the *ppm1g*$^{-/-}$ MEF cell lines had significantly reduced viability treated with either doxorubicin or H_2O_2. The increased cell death in the stressed *ppm1g*$^{-/-}$ MEFs illustrates the essential and cell-autonomous role of ppm1g for cell survival under stress stimulations.

Combining both *in vitro* and *in vivo* analyses as presented in this report, it is clear that PPM1G mediated signaling is a conserved and functionally important pathway for CNS

development. These observations provide the physiological context for the reported function of PPM1G in chromatin remodeling, RNA processing and DNA damage regulation.

Experimental Procedures

Animal welfare

All mice and zebrafish were housed and cared for by the staff of UCLA Division of Laboratory Animal Medicine according to current guidelines and policies set forth in Public Health Service Policy on Humane Care and Use of Laboratory Animals (2002). Euthanizing mice or zebrafish for tissue or cells was performed following specific protocols approved by UCLA Institutional Animal Care and Use Committee (UCLA Animal Research Committee protocol # 2003-105 for mice and 2000-051-33B for zebrafish).

ppm1g null mice

The *ppm1g*$^{-/-}$ mice were obtained from Deltagen. The *ppm1g*$^{-/-}$ allele was generated by fusing LacZ neomycin fusion gene cassette in-frame into the ppm1g coding sequences in exons 4 through exon 5 via homologous recombination. The cassette contains a stop codon, a polyA and strong splicing acceptor to stop transcript 3′ to the insert. *ppm1g*$^{+/-}$ mice were backcrossed into C57BL background. Mice were housed under standard conditions with a 12 hour light dark cycle. Heterozygous mice were crossed and the embryos were harvested at different embryonic developmental time points as indicated. Genotyping was performed on genomic DNA based on PCR as illustrated in Figure 1A. PCR product *ab* represents wildtype allele with 297bp in length and PCR product cb represents targeted allele with 585bp in length.

Primer a: 5′-CATGACTATTGAAGAGCTGCTGACG-3′

Primer b: 5′-TTAGCAACTCGAGGCAGCTTGTCAG-3′

Primer c: 5′-GGGCCAGCTCATTCCTCCCACTCAT-3′

β−galactosidase staining

For LacZ staining of embryos, dissected embryos were fixed in 2% gluteraldehyde in PBS for 10 minutes followed by incubation in staining solution containing 100 mM Na phosphate pH 7.4, 0.01% deoxycholate, 0.02% NP40, 5 mM potassium ferrocyanate, 5 mM potassium ferricyanate, 2 mM MgCl and 3 μg/ml Indigal at 37°C.

Zebrafish ppm1g and morpholino injection

Zebrafish colonies (AB strain) were cared for and bred under standard conditions. The developmental stages were determined using morphological features of fish raised at 28.5 °C (Westerfield, 2000). The zebrafish ppm1g (ACCESS Number: BC 052132) was cloned from a cDNA prepared from 2 pfd embryos using the following primers:

ppm1g-F: GGGGGCTTACTTGTCTCAACCCAA

ppm1g-R: TTACTCAGTTTTGGGTTTTTTGCTG

The cDNA fragment was then cloned into pCS2-myc vector for expression and riboprobe preparation. A morpholino antisense oligonucleotide (Gene-Tools) complementary to the translation start site of *ppm1g* and its flanking sequence (ppm1gMO, 5′-GAGACAAGTAAGCCCCCATGATGTG-3′) was synthesized. The lyophilized morpholino was reconstituted in 5mM HEPES, pH 7.6 at a concentration of 8 ng/nl. Wildtype AB embryos were injected with 6 or 8 ng of the ppm1gMO at the 1 cell stage.

In situ hybridization of zebrafish embryos

Embryos for in situ hybridization were raised in embryo medium supplemented with 0.2 mM 1-phenyl-2-thiourea to maintain optical transparency. Whole-mount *in situ* hybridization was performed as previously described (Langenbacher et al., 2011). Antisense *in situ* hybidization probes were generated from ppm1g (purchased from Open Biosystems), or from notch1b and pax2 plasmids as described (Nguyen et al., 2010).

Acridine orange staining

Live control and ppm1gMO injected embryos were soaked in the vital dye acridine orange (5 ug/ml in embryo medium) for 15 minutes. The embryos were then rinsed with embryo medium and viewed with an epifluorescence equipped Stemi SV 11 (Zeiss) using a GFP filter set. Images were captured with a Zeiss AxioCam and AxioVision software.

MEF Cells

Mouse embryonic fibroblasts (MEF) were derived from E10.5 embryos using an established protocol(Hogan, 1994). All cells were grown in DMEM media with 10% fetal bovine serum and 1% penicillin/streptomycin under 5% CO_2 at 37°C. All MEFs used in this study were immortalized with SV40T antigen as described(Lu et al., 2009).

qRT-PCR

Quantitative RT-PCR was performed on embryos to measure *ppm1g* mRNA expression. RNA was isolated from the embryos using the Trizol (Invitrogen) reagent according to standard protocols. One microgram of total RNA was reverse transcribed with iscript RT (Bio-Rad). qPCR was performed on a MyiQ™ Real-Time PCR Detection System (Bio-Rad) using ssofast evagreen polymerase (Bio-Rad). All results are reported as fold ct (cycle difference) change normalized to GAPDH from PCR reactions that were validated by both melting curve analysis and agarose gel electrophoresis. The following primers sets were used for qPCR:

ppm1g-F: GGACTAGCAGTCAACCGGAC

ppm1g-R: ACACAACAGAGCACAGGCAC

gapdh-F: TCCTGCACCACCAACTGCT

gapdh-R: GATGACCTTGCCCACAGCC

Immunohistochemistry and TUNEL staining

Paraffin embedded sections of embryos were utilized for immunohistochemistry and TUNEL staining. All samples were from stage-matched *ppm1g*$^{-/-}$ and control embryos. Immunohistochemistry was performed with antibodies against PH3 (Zymed) and counterstained with DAPI. TUNEL staining (Chemicon) was performed according to the manufacturer's instructions and counterstained with DAPI.

Immunoblot

Immunoblots were performed by separating proteins in Lysis Buffer (50 mM Tris-HCl pH 7.4, 150 mM NaCl, Triton X-100 1%, 1 mM EDTA, 1 mM EGTA, 2.5 mM Na pyrophosphate, 1 mM β−glycophosphate, 20 mM NaF, 1 mM Na orthovanadate, 1 mM PMSF and protease inhibitor tablet (Roche)) on 12% SDS PAGE gels that were transferred onto nitrocellulose membranes. The following antibodies were then used to probe the membranes: PPM1G (BD biosciences), actin (Santa Cruz), P-p38, p38α (Cell Signaling)

MTT assay for cell viability

MEF cells were cultured in 2% FBS DMEM for 48 hours prior to stimulation with 50 μM H2O2 or 1 μM Dox for 24 hours. Fresh 10% FBS DMEM containing 0.5 mg/ml MTT was added to cells for 15 minutes prior to washing and dye extraction with methyl sulfoxide. Absorbance was then measured at 650 nm. Two independent *ppm1g*$^{-/-}$ and *ppm1g*$^{+/+}$ MEF lines were used in this assay.

Statistical Analysis

For comparisons between *ppm1g*$^{-/-}$ and wild type, Student's t-test was employed. All error bars are standard deviation.

Supplementary Material

Refer to Web version on PubMed Central for supplementary material.

Acknowledgments

The authors wish to acknowledge outstanding technical assistance from Haiying Pu, technical help from Dr. Shahab Danesh and Dr. Jean-Louis Plouhinec. This work was in part supported by NIH Grants HL070079, HL103205, HL098954 and HL108186 for YW and UCLA Chancellor's Fellowship to WHF. No additional external funding received for this study

References

Allemand E, Hastings ML, Murray MV, Myers MP, Krainer AR. Alternative splicing regulation by interaction of phosphatase PP2Cgamma with nucleic acid-binding protein YB-1. Nat Struct Mol Biol. 2007; 14:630–638. [PubMed: 17572683]

Beli P, Lukashchuk N, Wagner SA, Weinert BT, Olsen JV, Baskcomb L, Mann M, Jackson SP, Choudhary C. Proteomic Investigations Reveal a Role for RNA Processing Factor THRAP3 in the DNA Damage Response. Mol Cell. 2012; 46:212–225. [PubMed: 22424773]

Elson A, Wang Y, Daugherty CJ, Morton CC, Zhou F, Campos-Torres J, Leder P. Pleiotropic defects in ataxia-telangiectasia protein-deficient mice. Proc Natl Acad Sci U S A. 1996; 93:13084–13089. [PubMed: 8917548]

Gabanella F, Carissimi C, Usiello A, Pellizzoni L. The activity of the spinal muscular atrophy protein is regulated during development and cellular differentiation. Hum Mol Genet. 2005; 14:3629–3642. [PubMed: 16236758]

Gu Y, Seidl KJ, Rathbun GA, Zhu C, Manis JP, van der Stoep N, Davidson L, Cheng HL, Sekiguchi JM, Frank K, Stanhope-Baker P, Schlissel MS, Roth DB, Alt FW. Growth retardation and leaky SCID phenotype of Ku70-deficient mice. Immunity. 1997; 7:653–665. [PubMed: 9390689]

Guthridge MA, Bellosta P, Tavoloni N, Basilico C. FIN13, a novel growth factor-inducible serine-threonine phosphatase which can inhibit cell cycle progression. Mol Cell Biol. 1997; 17:5485–5498. [PubMed: 9271424]

Hogan, B. Manipulating the mouse embryo : a laboratory manual. Plainview, N.Y.: Cold Spring Harbor Laboratory Press; 1994. p. xvii, 497

Humphrey E, Fuller HR, Morris GE. Current research on SMN protein and treatment strategies for spinal muscular atrophy. Neuromuscul Disord. 2011

Khoronenkova SV, Dianova II, Ternette N, Kessler BM, Parsons JL, Dianov GL. ATM-Dependent Downregulation of USP7/HAUSP by PPM1G Activates p53 Response to DNA Damage. Mol Cell. 2012; 45:801–813. [PubMed: 22361354]

Kimura H, Takizawa N, Allemand E, Hori T, Iborra FJ, Nozaki N, Muraki M, Hagiwara M, Krainer AR, Fukagawa T, Okawa K. A novel histone exchange factor, protein phosphatase 2Cgamma, mediates the exchange and dephosphorylation of H2A-H2B. J Cell Biol. 2006; 175:389–400. [PubMed: 17074886]

Komaki K, Katsura K, Ohnishi M, Guang Li M, Sasaki M, Watanabe M, Kobayashi T, Tamura S. Molecular cloning of PP2Ceta, a novel member of the protein phosphatase 2C family. Biochim Biophys Acta. 2003; 1630:130–137. [PubMed: 14654243]

Langenbacher AD, Nguyen CT, Cavanaugh AM, Huang J, Lu F, Chen JN. The PAF1 complex differentially regulates cardiomyocyte specification. Dev Biol. 2011; 353:19–28. [PubMed: 21338598]

Li J, Yang Y, Peng Y, Austin RJ, van Eyndhoven WG, Nguyen KC, Gabriele T, McCurrach ME, Marks JR, Hoey T, Lowe SW, Powers S. Oncogenic properties of PPM1D located within a breast cancer amplification epicenter at 17q23. Nat Genet. 2002; 31:133–134. [PubMed: 12021784]

Lu G, Sun H, She P, Youn JY, Warburton S, Ping P, Vondriska TM, Cai H, Lynch CJ, Wang Y. Protein phosphatase 2Cm is a critical regulator of branched-chain amino acid catabolism in mice and cultured cells. J Clin Invest. 2009; 119:1678–1687. [PubMed: 19411760]

Lu G, Wang Y. Functional diversity of mammalian type 2C protein phosphatase isoforms: new tales from an old family. Clin Exp Pharmacol Physiol. 2008; 35:107–112. [PubMed: 18197890]

Lu ZH, Books JT, Ley TJ. Cold shock domain family members YB-1 and MSY4 share essential functions during murine embryogenesis. Mol Cell Biol. 2006; 26:8410–8417. [PubMed: 16954378]

Murray MV, Kobayashi R, Krainer AR. The type 2C Ser/Thr phosphatase PP2Cgamma is a pre-mRNA splicing factor. Genes Dev. 1999; 13:87–97. [PubMed: 9887102]

Nguyen CT, Langenbacher A, Hsieh M, Chen JN. The PAF1 complex component Leo1 is essential for cardiac and neural crest development in zebrafish. Dev Biol. 2010; 341:167–175. [PubMed: 20178782]

Nussenzweig A, Chen C, da Costa Soares V, Sanchez M, Sokol K, Nussenzweig MC, Li GC. Requirement for Ku80 in growth and immunoglobulin V(D)J recombination. Nature. 1996; 382:551–555. [PubMed: 8700231]

Petri S, Grimmler M, Over S, Fischer U, Gruss OJ. Dephosphorylation of survival motor neurons (SMN) by PPM1G/PP2Cgamma governs Cajal body localization and stability of the SMN complex. J Cell Biol. 2007; 179:451–465. [PubMed: 17984321]

Rossoll W, Jablonka S, Andreassi C, Kroning AK, Karle K, Monani UR, Sendtner M. Smn, the spinal muscular atrophy-determining gene product, modulates axon growth and localization of beta-actin mRNA in growth cones of motoneurons. J Cell Biol. 2003; 163:801–812. [PubMed: 14623865]

Stern A, Privman E, Rasis M, Lavi S, Pupko T. Evolution of the metazoan protein phosphatase 2C superfamily. J Mol Evol. 2007; 64:61–70. [PubMed: 17160364]

Suh EJ, Kim YJ, Kim SH. Protein phosphatase 2Cgamma regulates the level of p21Cip1/WAF1 by Akt signaling. Biochem Biophys Res Commun. 2009; 386:467–470. [PubMed: 19538940]

Thisse B, Heyer V, Lux A, Alunni V, Degrave A, Seiliez I, Kirchner J, Parkhill JP, Thisse C. Spatial and temporal expression of the zebrafish genome by large-scale in situ hybridization screening. Methods Cell Biol. 2004; 77:505–519. [PubMed: 15602929]

Travis SM, Welsh MJ. PP2C gamma: a human protein phosphatase with a unique acidic domain. FEBS Lett. 1997; 412:415–419. [PubMed: 9276438]

Uchiumi T, Fotovati A, Sasaguri T, Shibahara K, Shimada T, Fukuda T, Nakamura T, Izumi H, Tsuzuki T, Kuwano M, Kohno K. YB-1 is important for an early stage embryonic development: neural tube formation and cell proliferation. J Biol Chem. 2006; 281:40440–40449. [PubMed: 17082189]

Westerfield, M. The Zebrafish Book. The University of Oregon Press; 2000.

Bullet points

-PPM1G is essentialfor mouse zebrafish embryonic development

-Loss of PPM1G leads to neuronal cell death and development defects in zebrafish and mice

-PPM1G regulates cell proliferation in vitro

-PPM1G regulates stress induced cell death in vitro

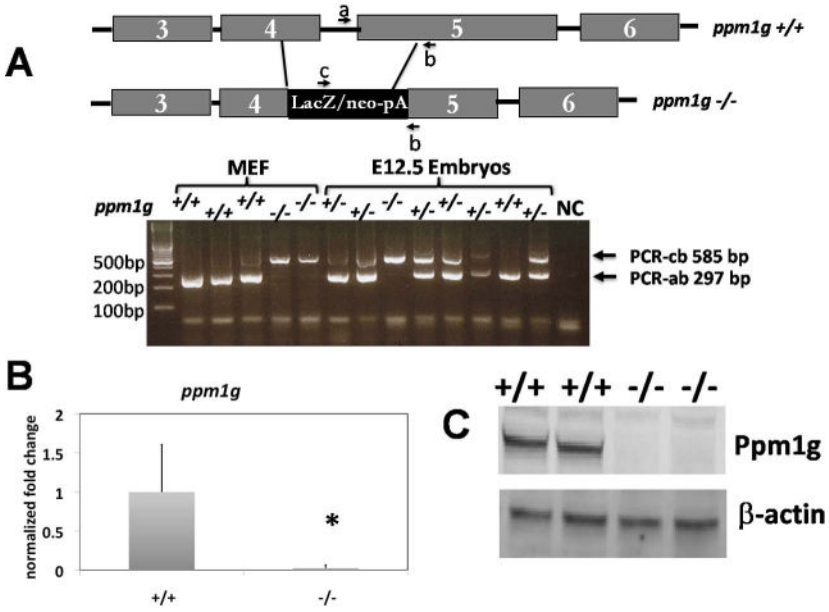

Figure 1. Genetic inactivation of *ppm1g* in mice

A. Schematics of the targeting gene construct where LacZ neomycin gene was inserted to replace part of *ppm1g* exons 4 and 5. The lower panel is a representative genomic DNA PCR result from MEF cells derived from $ppm1g^{-/-}$ and wildtype mouse embryos and on tissues from a litter of 12.5 day embryos resulted from a $ppm1g^{+/-} \times ppm1g^{+/-}$ cross as indicated. NC, no-DNA negative control. **B.** The relative *ppm1g* mRNA levels in wildtype or $ppm1g^{-/-}$ mouse embryos using qRT-PCR. Error bars indicate standard deviation, * $p < 0.05$. **C.** Immunoblots of PPM1G and β-actin protein in mouse embryonic fibroblasts derived from wildtype (+/+) and $ppm1g^{-/-}$ (−/−) embryos.

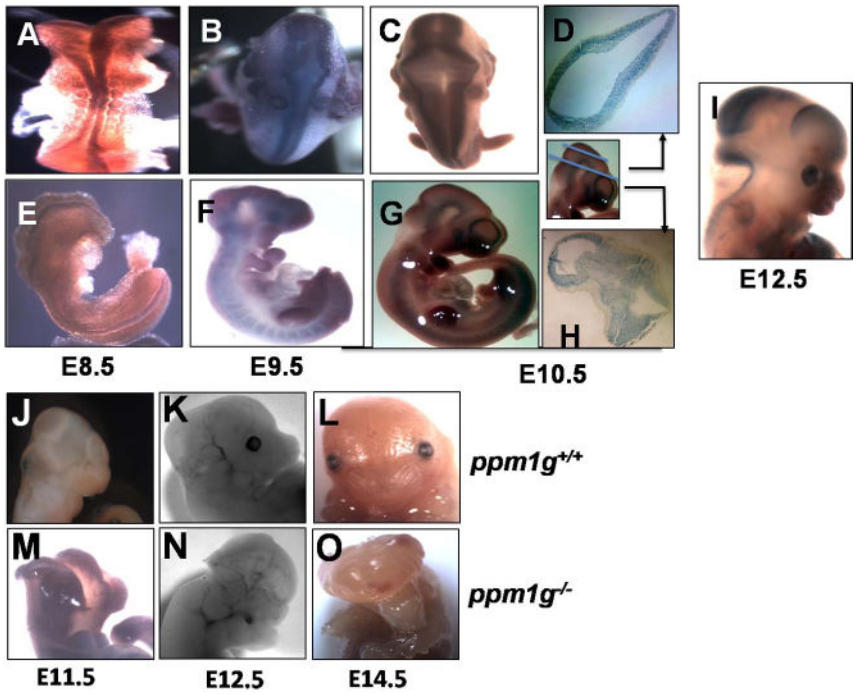

Figure 2.

Expression patterns of ***ppm1g*** and development of its inactivation in mice. *ppm1g*$^{+/-}$ embryos were stained for β–galactosidase as described in Methods. The whole mount *ppm1g* expression pattern was imaged for E8.5 (**A, E**), E9.5 (**B, F**), E10.5 (**C** and **G**) and E12.5 (**I**) embryos, also sections of brains were taken for E10.5 embryos (**D, H**) at the indicated locations. Gross morphology was imaged by a stereo dissecting microscope for *ppm1g*$^{+/+}$ (**J, K, L**) and *ppm1g*$^{-/-}$ (**M, N, O**) littermate embryos at E11.5, E12.5, and E14.5 as indicated.

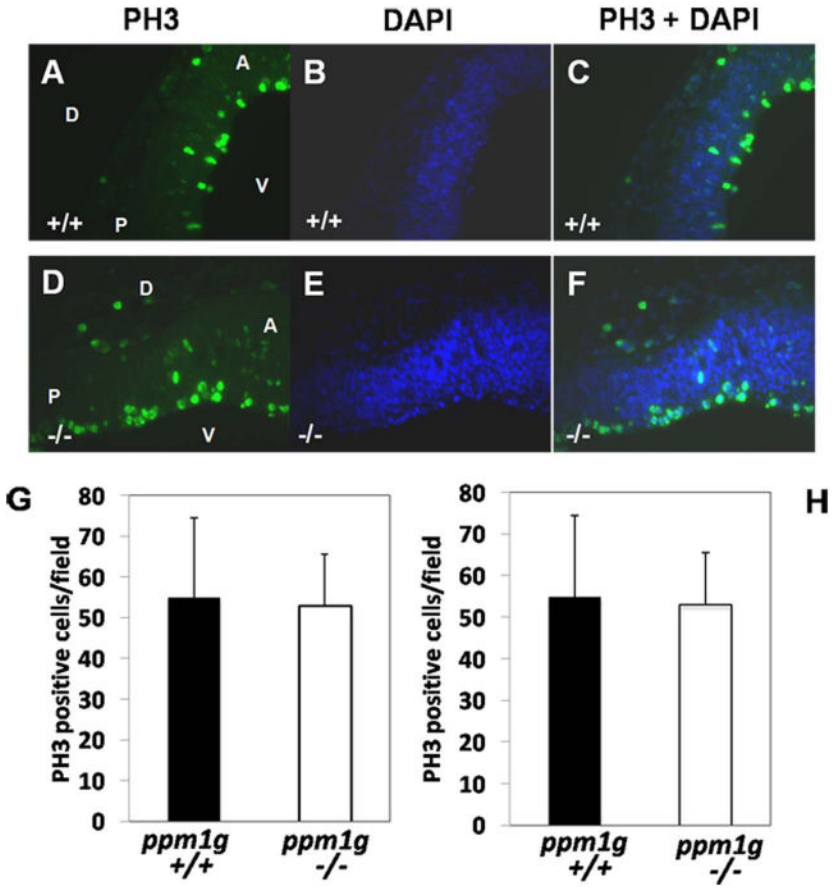

Figure 3. *ppm1g*$^{-/-}$ embryos have normal proliferation in the CNS

Sections through the midbrain of *ppm1g*$^{+/+}$ (**A–C**) and *ppm1g*$^{-/-}$ (**D–F**) were imaged with an immunofluorescent microscopy for phosphorylated Histone-3 (H3P) (**A, D**), DAPI (**B, E**) and overlaid images (**C, F**). v, ventricle side; d, dorsal side; a, anterior side; p, posterior side. **G**. PH3 positive cells per field between *ppm1g*$^{+/+}$ and *ppm1g*$^{-/-}$ embryos. n= 3 in each group.

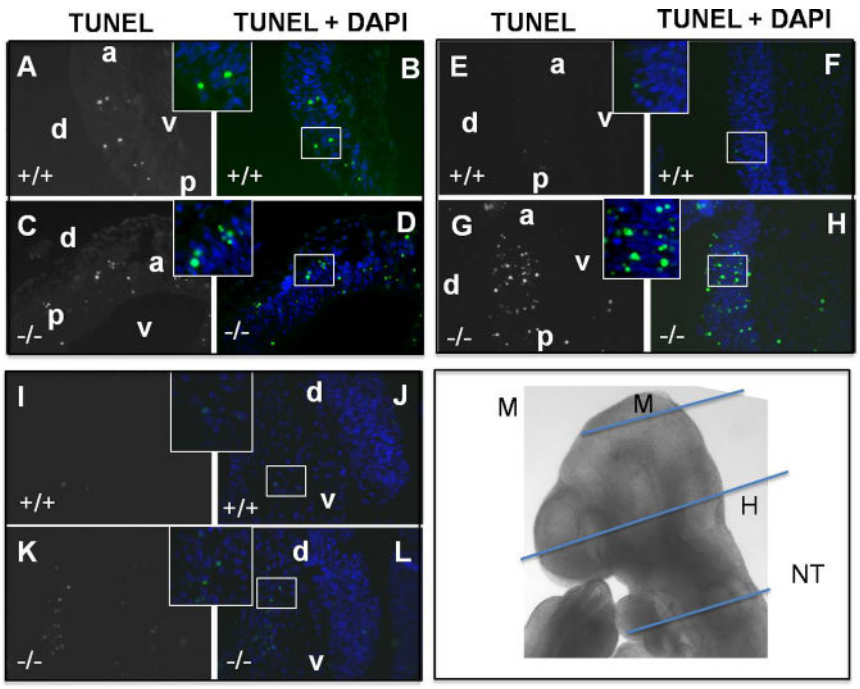

Figure 4. ***ppm1g*** $^{-/-}$ **embryos have increased apoptosis in the midbrain and hindbrain**

Sections through the midbrain (**A–D**), hindbrain (**E–H**) and neural tube (**I–L**) were TUNEL stained and counterstained with DAPI as indicated from E9.5 *ppm1g* $^{+/+}$ and *ppm1g* $^{-/-}$ embryos (**M).** The general locations of the sections for midbrain (M), hindbrain (H) and neural tube (NT). v, ventricle side; d, dorsal side; a, anterior side; p, posterior side. The inserts are enlarged from image areas as indicated.

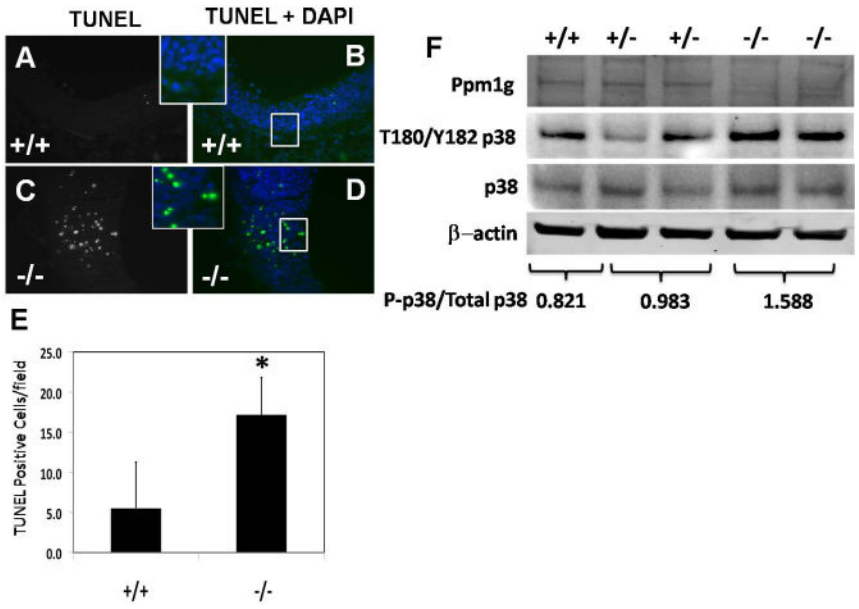

Figure 5. E10.5 *ppm1g*$^{-/-}$ embryos have augmented midbrain apoptosis and stress signaling

A–D TUNEL staining of E10.5 embryos midbrain sections from *ppm1g*$^{+/+}$ and *ppm1g*$^{-/-}$ embryos. **E**. Quantification of TUNEL positive cells between *ppm1g*$^{+/+}$ and *ppm1g*$^{-/-}$ embryos, Error bars indicate standard deviation. *p<0.05. **F.** Immunoblot for phospho- and total p38 in E10.5 embryos from *ppm1g*$^{-/-}$, *ppm1g*$^{+/-}$ and *ppm1g*$^{+/+}$ as indicated. Inserts are enlarged from image areas as indicated.

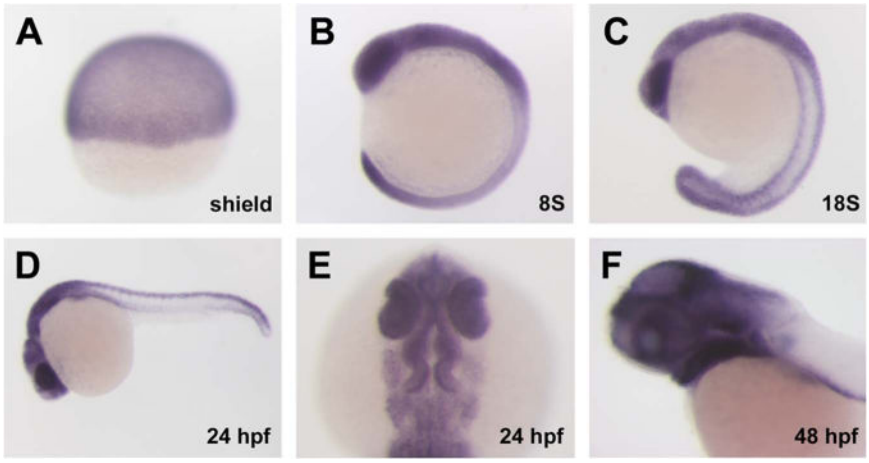

Figure 6. *ppm1g* expression pattern during zebrafish embryonic development

ppm1g mRNA was detected by *in-situ* hybridization at different developmental stages from the onset of gastrulation (**A**) to somitogenesis (**B,C**). Strong expression is shown in the brain, spinal cord, eyes, and branchial arches at both 24 hours post fertilization (hpf) (**D**, lateral; **E**, dorsal) and 48 hpf (**F**).

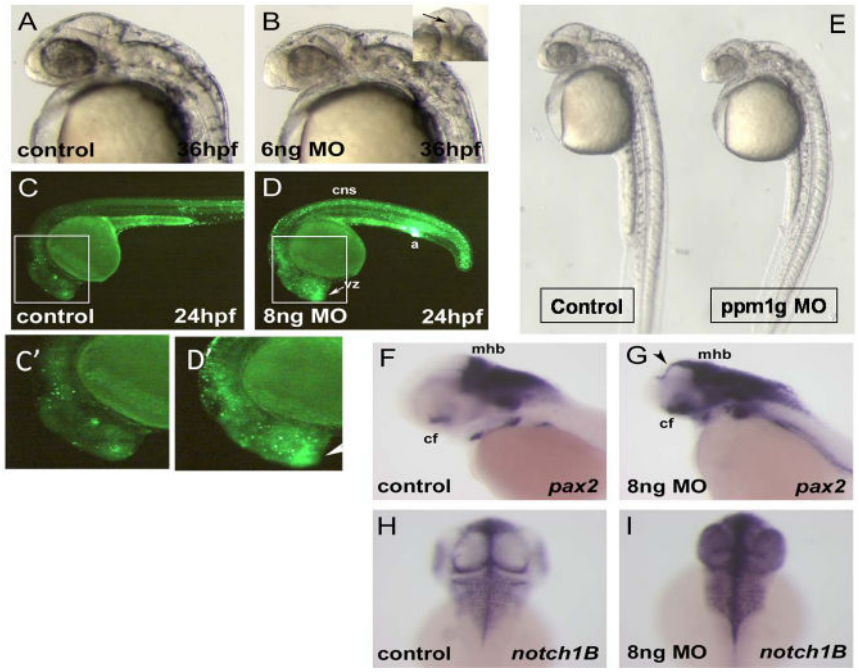

Figure 7. *ppm1g* morphants have central nervous system defects and aberrant expression of brain markers

A–B. Morphology of embryos injected with 6ng *ppm1gMO* or control at 36hpf. Morphants also have necrotic tissue in the presumptive telencephalon (B, inset). **C–D**. Acridine orange staining indicates elevated apoptosis in the forebrain ventricular zone (vz), central nervous system (cns), and anus (a) in the *ppm1g* morphants at 24 hpf. C′ and D′ are inserts enlarged from image areas in C and D as indicated. In-situ hybridization signal for pax2 in *ppm1g* morphant and control. **F–G**. Abnormal expression of pax2 in the *ppm1g* morphant was identified in the midbrain tectum (arrowhead), choroid fissure (cf) and optic nerve. **H–I**. Dorsal view of in situ hybridization signal for notch1B in the *ppm1g* morphant and control.

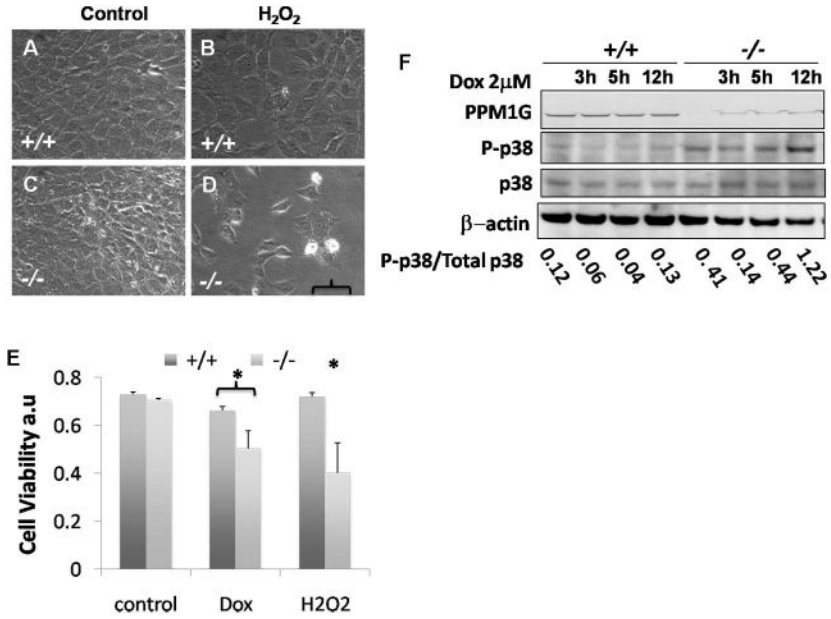

Figure 8. *ppm1g* regulates cell survival

A–D. Cellular morphology and viability of *ppm1g*$^{+/+}$ and *ppm1g*$^{-/-}$ MEFs treated with vehicle or 50 μM H_2O_2 for 24 hours. **E.** Relative cellular viability measured by MTT assay on *ppm1g*$^{+/+}$ and *ppm1g*$^{-/-}$ MEFs treated with 1μM Dox or 50 μM H_2O_2 for 24hrs. Error bars indicate standard deviation, * $p < 0.05$. **F.** Immunoblots for PPM1G, *ppm1g*$^{+/+}$ and *ppm1g*$^{-/-}$ MEFs were treated with Dox for 3, 5 or 12 hours as indicated and analyzed by immunoblot for stress activated p38 activation.

Table 1

Embryonic lethality in *ppm1g*$^{-/-}$ mice

ppm1g$^{+/-}$ mice were crossed and the resulting embryos of mice of different genotypes are listed along with the percentage of *ppm1g*$^{-/-}$ embryos.

	+/+	+/−	−/−	% −/−	total
8.5	3	8	3	21.4	14
9.5	6	17	6	20.7	29
10.5	65	119	36	16.4	220
12.5	24	36	11	15.5	71
13.5	24	28	5	8.8	57
14.5	22	15	1	2.6	38
15.5	3	6	0	0	9
19.5	3	5	0	0	8
P0	20	34	0	0	54
weaned	61	76	1	0.72	138
	+/+	+/−	−/−		
total	251	364	73		688